Impact of Coherent Ocean Stratification on AMOC Reconstruction by Coupled Data Assimilation with a Biased Model

9 authors, including:

Lv Lu
Ocean University of China
4 PUBLICATIONS   **10** CITATIONS

SEE PROFILE

Stephen G Yeager
National Center for Atmospheric Research
109 PUBLICATIONS   **7,742** CITATIONS

SEE PROFILE

S. Zhang
National Oceanic and Atmospheric Administration
86 PUBLICATIONS   **2,176** CITATIONS

SEE PROFILE

Ping Ping Chang
National Taiwan Normal University
169 PUBLICATIONS   **7,307** CITATIONS

SEE PROFILE

Some of the authors of this publication are also working on these related projects:

Coordinated Ocean-ice Reference Experiments View project

AMOC; data assimilation View project

Impact of Coherent Ocean Stratification on AMOC Reconstruction by Coupled Data Assimilation with a Biased Model

Lv Lu,[a] Shaoqing Zhang,[a,b,c,d] Stephen G. Yeager,[c,e] Gokhan Danabasoglu,[c,e]
Ping Chang,[c,f] Lixin Wu,[a,b,c,d] Xiaopei Lin,[a,b,c,d] Anthony Rosati,[g] and Feiyu Lu[g,h]

[a] Key Laboratory of Physical Oceanography, Ministry of Education, and Ocean University of China, Qingdao, China
[b] Function Laboratory for Ocean Dynamics and Climate/Pilot National Laboratory for Marine Science
and Technology (QNLM), Qingdao, China
[c] International Laboratory for High-Resolution Earth System Prediction (iHESP), College Station, Texas
[d] College of Oceanic and Atmospheric Sciences, Ocean University of China, Qingdao, China
[e] National Center for Atmospheric Research, Boulder, Colorado
[f] Department of Oceanography, Texas A&M University, College Station, Texas
[g] Geophysical Fluid Dynamics Laboratory, National Oceanic and Atmospheric Administration, Princeton, New Jersey
[h] Program in Atmospheric and Oceanic Sciences, Princeton University, Princeton, New Jersey

ABSTRACT

The Atlantic meridional overturning circulation (AMOC) is of great importance in Earth's climate system, and reconstructing its structure and variability by combining observations with a coupled model is a key step in understanding historical and future states of AMOC. However, models always have systematic errors called bias owing to imperfect numerical representation of the real world. Model bias and the sparse nature of ocean observations, particularly in deep oceans, make it difficult to generate a complete historical picture of AMOC structure and variability. Here, two coupled models that are biased with respect to each other are used to design "twin" experiments to systematically study the influence of model bias on AMOC reconstruction. One model is used to produce the "observations" that sample the "true" solution of the AMOC to be reconstructed, while the other model is used to incorporate the "observations" to reconstruct the "truth" through coupled data assimilation (CDA). The degree to which the "truth" is recovered by a CDA scheme assesses the critical role of coherent (both upper- and deep-ocean incorporate enough observations to mitigate stratification instability) ocean stratification on AMOC reconstruction. Results show that balancing restoration of climatology and assimilation of observations is vital to better reconstruct AMOC structure and variability, given that most ocean observations are only available in the upper 2000 m. The gained results serve as a guideline in ocean-state estimation with a balance of deep restoring and upper data constraint for climate prediction initialization, especially for decadal predictions.

1. Introduction

The Atlantic meridional overturning circulation (AMOC) with the northward (southward return) flow in the upper (deep) Atlantic is a significant part of Earth's climate system (Delworth et al. 2008). In the Atlantic, the AMOC transports more than 1 PW of heat from south of the equator to high latitudes (Johns et at. 2011; Macdonald and Baringer 2013), attributable to the slightly warmer North Hemisphere than the Southern Hemisphere, as well as to the mean position of the intertropical convergence zone being north of the equator (e.g., Frierson et al. 2013; Marshall et al. 2014; Buckley and Marshall 2016).

Given the short period of direct observations, our understanding of AMOC largely comes from model studies. Karspeck et al. (2015) compared the behavior of the AMOC in various ocean and coupled reanalysis products, and found that there are significant differences in both AMOC structure and variability among the products, despite their use of similar observational constraints. For example, although the AMOC structure in the Geophysical Fluid Dynamics Laboratory (GFDL) coupled model (Fig. 1a) has a somewhat similar pattern as in the ECMWF ORAS4 (Fig. 1c), the mean transports are stronger in ORAS4 and variability of the two analysis products is quite different (Figs. 1b,d). Large variability in the GFDL model (Fig. 1b) occuring in the deep ocean at the equatorial area may be associated with the

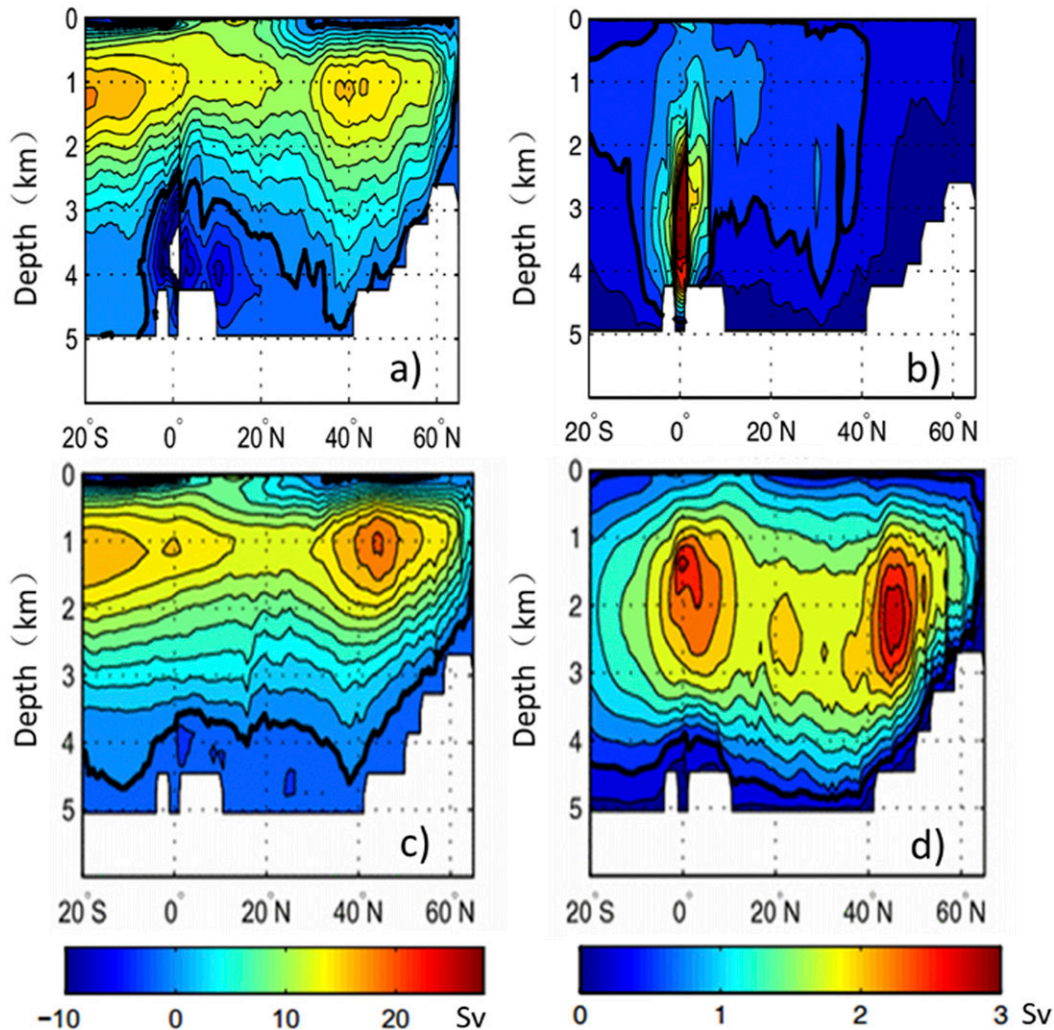Corresponding author: Shaoqing Zhang, szhang@ouc.edu.cn

Fig. 1. Reconstructed AMOC (left) mean states and (right) standard deviation of the annual-mean, linearly detrended streamfunction in (a),(b) GFDL ECDA and (c),(d) ECMWF ORAS4 products. Bold line is the zero contour for mean states and 0.5-Sv contour for standard deviation. Contour interval is 2 Sv for mean states and 0.25 Sv for standard deviation. From Karspeck et al. (2015).

climatological restoring (Karspeck et al. 2015). Also, the lower cell is weak in ORAS4 and the ensemble coupled data assimilation (ECDA) system shows a strong deep equatorial counterclockwise circulation. Although the recent analysis of more ocean/coupled reanalysis products by Jackson et al. (2019) showed more agreement on overall AMOC characteristics, especially the weakening trend in the historical simulation, distinct differences in structure (see Fig. 2 of Jackson et al. 2019) and variability (see Fig. 11 of Jackson et al. 2019) exist. These differences in AMOC structure and variability in different models and reanalysis products, for which the inherent model bias plays an important role (Dee and da Silva 1998; Dee 2004, 2005), lead to large uncertainties in representation and understanding of the AMOC.

The general adverse impact of model bias on data assimilation has been widely studied (e.g., Dee and da Silva 1998; Balmaseda et al. 2007; Dee 2005; Zhang and Rosati 2010; Zhang et al. 2014). The model bias generally refers to the systematic difference (or called error) between model simulations and observations, resulting from the misfitting of model dynamical core and physical processes (e.g., Zhang et al. 2012). Although the model bias could consist of errors in mean state and variability spectral structure, it is the mean-state error, which is a major obstacle to data assimilation, that is generating artifacts in analyzed variability (e.g., Dee and da Silva 1998; Dee 2004, 2005). Direct statistical correction has been applied to ocean data assimilation (ODA) to address the adverse impact of ocean model

bias on ocean-state analysis (e.g., Chepurin et al. 2005; Balmaseda et al. 2007). Zhang and Rosati (2010) designed an adaptively inflated scheme to relax the influence of coupled model bias on deep-ocean-state estimation within a "twin" experiment framework using two coupled models with an identical ocean model component. This study tends to use two independent coupled models to thoroughly examine the adversely impact of coupled model bias (mean-state error) on AMOC reconstruction, in which both the atmosphere and ocean models in the assimilation model and observational model are entirely different.

As the AMOC is a product of atmosphere–ocean coupling, and observations are sparse in both space and time (particularly sparse in the deep ocean due to measuring difficulties), model bias makes it especially challenging to reconstruct AMOC structure and variability by combining coupled models with observations in maintaining the coupling mechanism. For example, the sparse and discontinuous nature of observations means that the bias of a given model is not a well-defined quantity. In addition, the AMOC is an integration of the wind-driven circulation and three-dimensional oceanic thermohaline structures, for which the long-term mean structure and variability are not directly observable. These factors make it difficult to evaluate the quality of a reconstructed AMOC. For example, it would be difficult to argue which one is better in Fig. 1.

Understanding the influence of model bias on AMOC reconstruction within an idealized framework using the sea surface temperature (SST) and Argo ocean observing network is a key step toward accurately reconstructing the structure and variability of AMOC. In this study, we design a twin experiment framework with two coupled models that are biased with respect to each other. Although these two models also have a different representation of variability, we particularly use the framework to address the issue of model bias. In such a framework, one coupled model is used to represent the "true" solution of the coupled data assimilation (CDA) problem, from which the "observations" [sampling the model simulation results onto the in situ data network, the SST, and Argo profiles, in this case; described in section 2b(2)] are sampled. The other coupled model is used to conduct CDA for incorporating the "observations" into the model to recover the "truth." The resulting AMOC structure and variability represents a reconstruction by combining a biased coupled model with "observations." The degree to which the AMOC structure and variability of the "truth" is recovered with a bias-counted CDA scheme is an assessment of the influence of model bias on AMOC reconstruction. Our focus is on the influence of biased ocean stratification on the reconstructed mean structure and variability of AMOC.

The remainder of this paper is organized as follows. Section 2 presents methodology, including brief descriptions for the two coupled models, NCAR CESM1.3 and GFDL CM2.1, and the CM2.1-ECDA system. Section 3 presents the problems associated with the reconstructed AMOC using the traditional CDA scheme if the ocean model bias is not appropriately handled. Section 4 presents the results of various CDA schemes that use global restoring to the climatology derived from the "truth" model to enhance stability of the ocean stratification. Finally, an optimal CDA scheme among three with appropriate climatological restoring and instantaneous data constraints for best retrieving the AMOC structure and variability is discussed and analyzed. Discussions and conclusions are given in section 5.

2. Methodology

a. Coupled models and coupled data assimilation

We use the Community Earth System Model version 1.3 (CESM1.3)—an updated version from Hurrell et al. (2013)—developed at the National Center for Atmospheric Research (NCAR) as the "truth" model to produce "observations," and the GFDL second-generation coupled model (CM2.1) (Delworth et al. 2006; Gnanadesikan et al. 2006) as the target model that assimilates the "observations" to recover the "truth" by a CDA approach. The corresponding CDA method is the ensemble coupled data assimilation system based on CM2.1 (CM2.1-ECDA) (Zhang et al. 2007; Zhang and Rosati 2010).

1) NCAR CESM1.3

CESM1.3 is a fully coupled global Earth system model that provides most advanced simulations of Earth's climate states for various time period. A similar version of the model was used in simulations participating in phase 5 of the Coupled Model Intercomparison Project (CMIP5) (Taylor et al. 2012). In this study, we conducted a historical (transient) simulation (so-called BHISTC5, a historical setting of CAM5 starting from 1850 as the atmosphere model) in which the components include the Parallel Ocean Program version 2 (POP2) for ocean, the Community Atmosphere Model version 5 (CAM5) for atmosphere, the Community Land Model version 4.0 (CLM4.0) for land, and the Community Ice Code (CICE) for sea ice. POP2 has an approximately $1° \times 1°$ horizontal (latitude–longitude) resolution with meridional resolution on the order of $0.3°$ near the equator (the same as CICE) with 60 vertical layers, while CAM5 has a horizontal resolution of $1.9° \times 2.5°$ (the same as CLM4.0) with 32 vertical levels.

As described above, CESM1.3 is used in this work to define the "true" solution for climate reconstruction in the twin experiment framework, providing the "observations."
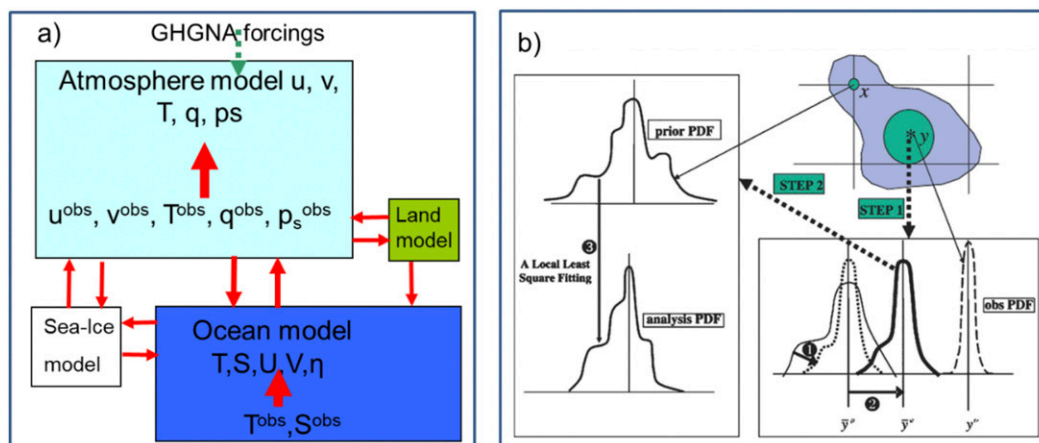
FIG. 2. Cartoon of how (a) the observations in components of an atmosphere (land) and ocean (sea ice) coupled model impact model variables (denoted by the thick red arrows) and model components interact with each other by exchanging fluxes (red arrows), and (b) an ensemble filter updates the probability distribution for a scalar variable given an observation. The dashed green arrow in (a) denotes the radiative forcings expressed by the atmospheric greenhouse gas and natural aerosol (GHGNA) and means that the GHGNA radiative forcings in assimilation may be set as a preindustrial fixed year or with historical records. The upper left of (b) represents the prior distribution derived from model ensemble integrations starting from the previous assimilation results. The upper right of (b) represents an observation available at the location denoted by the asterisk with a Gaussian distribution at the lower right, which leads the ensemble spread adjustment (shown by ①) and the ensemble mean shift (shown by ②). A filtering process, shown by ③ at the left of (b), combines the observational and prior distributions to form an analyzed distribution [lower left of (b)] realized by a set of adjusted ensemble members, which are initial conditions for the next ensemble integrations. Here ① + ② implements step 1 and ③ carries out step 2 of the two-step adjustment described in section 2a(3).

2) GFDL CM2.1

By combining the atmosphere model 2.1 and land model 2.1 (AM2.1–LM2.1) with version 4 of the Modular Ocean Model (MOM4) and the Sea Ice Simulator (SIS), the GFDL of the National Oceanic and Atmospheric Administration (NOAA) has developed the second generation of the fully coupled general circulation Climate Model, version 2.1 (CM2.1), for use of its simulations in the Intergovernmental Panel on Climate Change (IPCC) Fourth Assessment Report (AR4) (Randall et al. 2007). The atmospheric model AM2.1 is based on a finite-volume dynamical core (Lin 2004), has a horizontal resolution of 2.0° × 2.5° (the same as LM2.1), and 24 vertical levels. MOM4 has 50 vertical levels (10-m thickness per layer for top 22 levels) and 1° × 1° horizontal resolution refining to 1/3° near the equator in the meridional. GFDL CM2.1 is also run in the historical configuration.

3) COUPLED DATA ASSIMILATION SYSTEM: CM2.1-ECDA

The bias-counted data assimilation scheme of this study, which directly addresses the model bias issue, starts from the ensemble coupled data assimilation system (CM2.1-ECDA) using the ensemble adjustment Kalman filter (EAKF) (Anderson 2001, 2003) with an inflated coupled ensemble filtering scheme (Zhang and Rosati 2010). The inflated ECDA system enhances the subsurface observational constraint through inflating the ensemble spread in the filtering regression, thus relaxing influences of ocean model bias on ODA to some degree. Detailed information on CM2.1-ECDA is available in Zhang et al. (2007, 2010). Here, we only comment on relevant aspects to this study. As in these referenced previous studies, the CDA used here is a weakly coupled data assimilation scheme (illustrated by Fig. 2a), in which the oceanic (atmospheric) observations only directly adjust the ocean (atmosphere) component of the coupled model while the exchange fluxes of coupled model can transfer the observational information between the model components.

The adaptively inflated ensemble Kalman filter (Zhang and Rosati 2010) is implemented using a two-step local least squares filtering (Anderson 2003). With a Gaussian approximation for the model background uncertainties, the first step calculates the observational increment through convolution of two Gaussians (as shown in the right part of Fig. 2b). After a few standard manipulations (e.g., Zhang et al. 2007) illustrated by the steps 1 and 2 in Fig. 2b (encircled numbers), the observational increment for the ith ensemble member produced by the kth observation $\Delta y^o_{i,k}$ is calculated as

$$\Delta y_{i,k}^o = \frac{\overline{y}_k}{1 + \kappa^2(y_k, y_k^o)} + \frac{y_k^o}{1 + \kappa^{-2}(y_k, y_k^o)}$$
$$+ \frac{y_{i,k} - \overline{y}_k}{\sqrt{1 + \kappa^2(y_k, y_k^o)}} - y_{i,k}, \tag{1}$$

where the first two and the third terms at the right-hand side of the equation stand for the ensemble mean shift (denoted by ② in Fig. 2b) and the ensemble spread adjustment (denoted by ① in Fig. 2b), respectively. Also, y_k with an overbar denotes the mean of model ensemble estimate for the observation y_k^o at the observational location k denoted as $y_{i,k}$; $\kappa(y_k, y_k^o)$ represents the ratio of standard deviations of model ensemble spread and observational errors at location k (i.e., σ_k/σ_k^o). Under the assumption of perfect model, the increment in Eq. (1) is only related to forecast error variances, not referring to the systematic error of the model (bias).

The second step projects the observational increment onto the model grids through a least squares fitting (regression) using the ensemble statistics (as denoted by the left part of Fig. 2b) with the addition of the deep-ocean inflation scheme (Zhang and Rosati 2010), which to some extent addresses the ocean model bias. As in Zhang and Rosati (2010), considering localization and deep-ocean inflation, the regression of any oceanic variable at grid point j for the ith ensemble member $x_{i,j}$ with the observation increment calculated by Eq. (1) can be expressed as

$$\Delta x_{i,j} = \Omega_{j,k} \rho(x_j, y_k) \Delta_{i,k}(\kappa, \kappa_0, \Delta y_{i,k}^o, \Delta y_{i,k,0}^o), \tag{2}$$

where $\Delta_{i,k}$ is a function of κ, κ_0, $\Delta y_{i,k}^o$, and $\Delta y_{i,k,0}^o$ [see Eq. (3) of Zhang and Rosati 2010], representing a combination of adjusted increments (before weighted by correlation and localization) computed by applying the model ensemble statistics (producing κ and $\Delta y_{i,k}^o$) and historical data statistics (producing κ_0 and $\Delta y_{i,k,0}^o$). The terms κ and κ_0 are the ratios of the standard deviations of model variables x_j (being adjusted at grid point j) and y_k (being observed at location k), respectively, as estimated by the model ensemble (for κ) and adaptively updated "historical" data (for κ_0), representing stationary and flow-dependent error statistics, while $\Delta y_{i,k}^o$ and $\Delta y_{i,k,0}^o$ are the resulting observational increments applying κ and κ_0 to Eq. (1), respectively, and ρ is the correlation coefficient between x_j and y_k. The term $\Omega_{j,k}$ is the covariance localization function (see Zhang et al. 2005), which is only determined by the distance between locations j and k. For more details, please refer to Zhang and Rosati (2010).

Combining the inflated ECDA system described above with climatology restoring, this study designs a bias-counted ODA scheme to directly address the model bias issue of the entire ocean and examine its impact on the AMOC reconstruction.

b. Experimental design

1) BIASED TWIN EXPERIMENTS

In this part, we introduce a biased twin experiment framework in which CESM1.3 is the "observational" (TRUTH) model while CM2.1 is the assimilation (biased) model. The "true" solution of the reconstruction problem (denoted as TRUTH) is a priori defined by a historical simulation of the CESM1.3 model from 1850 to 1999. The 20-yr period from 1978 to 1997 was set as the target for the reconstruction, which produces the synthesis "observations." As a contrast, a free control (CTL) experiment without any data constraint serving as a reference of assimilation is first conducted using CM2.1 initialized from the states of a historical simulation at 0000 UTC 1 January 1978 until 31 December 1997. Starting at 0000 UTC 1 January 1978, we run 11-day CTL to obtain 12 daily departure atmosphere restarts combined with the ocean initial condition of CTL as the 12-member initial conditions of the CM2.1-ECDA system. Then we try to recover the "TRUTH" in this 1978–97 period with the assimilation of atmospheric and/or oceanic data. To reconstruct AMOC using this "biased" CM2.1 (vs. CESM1.3) coupled model, we first conducted a basic CDA experiment (called CDA₀) to examine the deficiencies of the reconstructed AMOC mean state and variability. Further CDA experiments were then designed to improve the result. All model simulations and assimilation experiments are listed in Table 1.

2) DATA

In the experiments, we use regridded CESM1.3 atmospheric wind and temperature data (converted to the same grid as CM2.1 on all level), Argo data, and gridded SST (both derived from CESM1.3 simulation). The atmospheric "observations" from CESM1.3 take the gridded reanalysis format of temperature and wind superimposed by a random white noise with respective standard deviations of $1\,\mathrm{K}$ and $1\,\mathrm{m\,s}^{-1}$, and 6-h time intervals. The ocean "observations" are produced by sampling the "truth" (i.e., the 1978–97 model states of the CESM1.3 historical run) ocean temperature and salinity onto the 2007 Argo network repeatedly (as shown in Fig. 3), as well as gridded daily SST data. The ODA frequency is daily to assimilate Argo profiles and SST data. A 4-day observational window is applied for Argo profiles. Following the previous OSSE (Observing

TABLE 1. List of experiments.

Expt	Model	Initial condition	Forcing	Data constraint	Period
TRUTH	CESM1.3	Start from 1850 of BHISTC5 case	BHISTC5 case 1850–2000 radiative forcings	Free run	1850–2000
CTL	CM2.1	Historical simulation (member 1) at 0000 UTC 1 Jan 1978	Historical radiative forcings	Free run	1978–97
CDA_0	CM2.1	As in CTL	As in CTL	Traditional CDA	1978–87
$Restoring_1$	CM2.1	As in CTL	As in CTL	Restoring below 1000 m	1978–80
CDA_1	CM2.1	From $Restoring_1$ at 0000 UTC 1 Jan 1981	As in CTL	CDA + $Restoring_1$	1981–87
$Restoring_2$	CM2.1	As in CTL	As in CTL	Restoring below 0 m	1978–80
CDA_2	CM2.1	From $Restoring_2$ at 0000 UTC 1 Jan 1981	As in CTL	CDA + $Restoring_2$	1981–97
$Restoring_3$	CM2.1	As in CTL	As in CTL	Restoring below 0 m but different restoring coefficient	1978–80
CDA_3	CM2.1	From $Restoring_3$ at 0000 UTC 1 Jan 1981	As in CTL	CDA + $Restoring_3$	1981–97

System Simulation Experiment) design (Zhang et al. 2007, 2010), the standard deviation of ocean observational errors is set as 0.5°C for temperature and 0.1 PSU for salinity at the surface, decaying gradually with a 2000-m e-folding depth to simulate the property of observational representativeness errors. In the Argo network, the number of salinity profiles is almost equal to that for temperature; for example,

the sum of temperature (salinity) profiles is 16 255 (16 126) in January 2007.

3. Problems in reconstructing the AMOC using traditional coupled data assimilation

First, we examine the different characteristics of AMOCs produced by the "truth" model (CESM1.3)
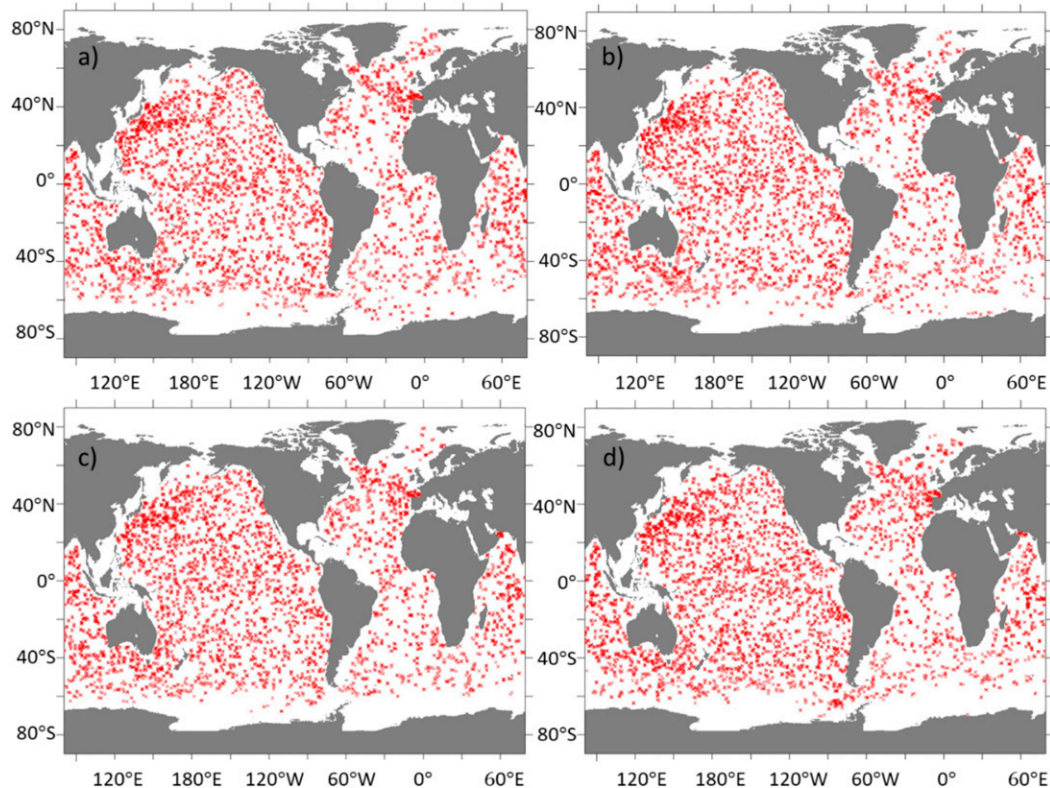
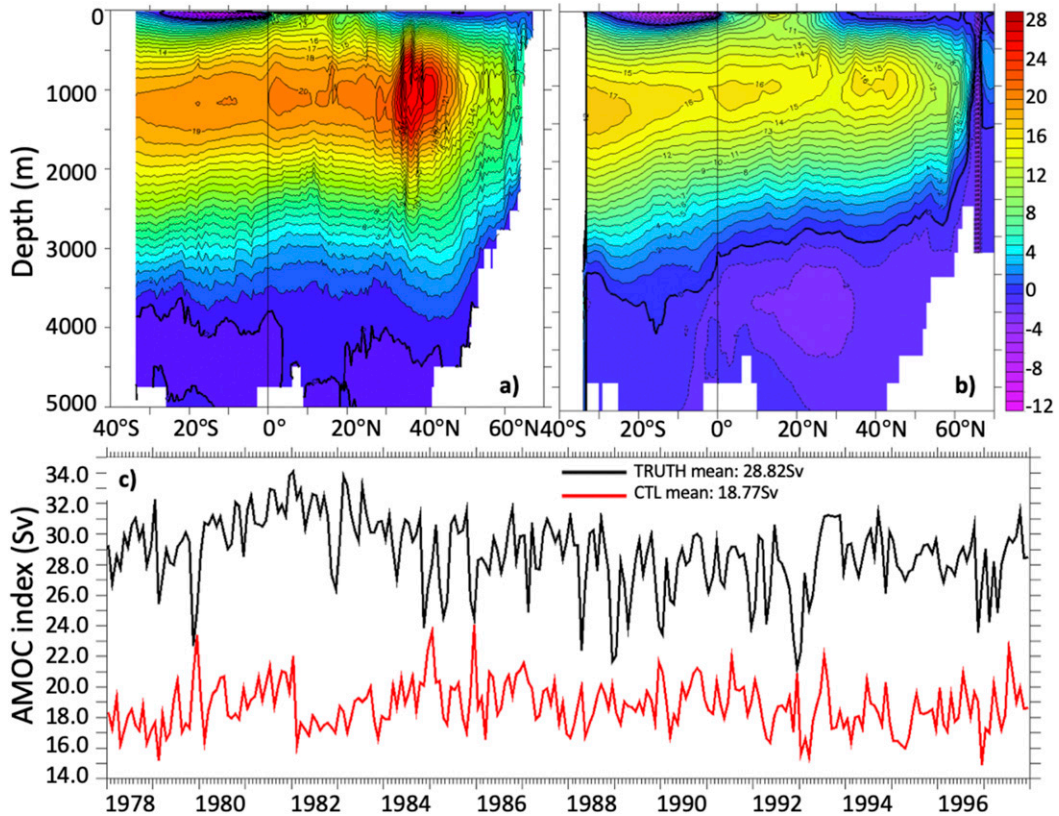FIG. 3. All Argo profiles in (a) January, (b) April, (c) July, and (d) November 2007.

FIG. 4. The AMOC (a),(b) mean state based on the CESM and CM2.1 historical simulations, respectively, and (c) monthly mean variability for the period of 1978–97.

and the biased model (CM2.1). As in many previous studies (e.g., Delworth et al. 1993, 2002; Keenlyside et al. 2008; Zhang et al. 2010; Yeager et al. 2014), an AMOC streamfunction (in Sv; $1\,\mathrm{Sv} = 10^6\,\mathrm{m}^3\,\mathrm{s}^{-1}$) is defined as the zonally integrated volume transport (see Karspeck et al. 2015), expressed as

$$\Psi(y, z) = \int_z^{\eta} \int_{x_{\mathrm{west}}}^{x_{\mathrm{east}}} v(x, y, z')\, dx\, dz', \tag{3}$$

where v is the meridional velocity, y is the latitude, z is the depth, η is the height of ocean surface, and x_{east} and x_{west} are the east and west boundaries of the Atlantic, respectively. To facilitate the comparison between the results of two models, we define the AMOC index as the maximum value of the AMOC streamfunction $\Psi(y, z)$ at the fixed latitude of 40°N (e.g., Mahajan et al. 2011) instead of the maximum value between 20° and 70°N (e.g., Delworth et al. 1993).

The AMOC time-mean streamfunctions from the CESM1.3 and CM2.1 CTL historical simulations, as well as time series of the corresponding monthly mean indices, are shown in Fig. 4. The broad structural features in

the AMOC mean states produced by both models have some similarities. For example, the upper cell (above ~3500 m) of AMOC includes northward surface flow and southward return flow of the North Atlantic Deep Water (NADW). The lower cell (below ~3500 m) represents the flow of the dense Antarctic Bottom Water (AABW). However, systematic differences between the two models are evident. First, compared with the CM2.1 AMOC, the CESM1.3 AMOC is on the whole much stronger, with a broader vertical extent of the NADW cell and much larger transport values. While the maximum transport magnitudes of the NADW cell to the south of 30°N in the CESM1.3 AMOC are above 20 Sv, the corresponding CM2.1 magnitude is 16–17 Sv. Notably, the maximum streamfunction in the strong overturning core between 30° and 50°N is ~19 Sv in CM2.1 but up to 29 Sv in CESM1.3. The value 29 Sv is higher than the typical CESM AMOC index due to the model spinup (the ocean model is initialized from Levitus data with modifications in the Arctic Ocean; Levitus et al. 1998; Steele et al. 2001; Danabasoglu et al. 2014), but such differences are not important for our present purposes, since we do not know the magnitude
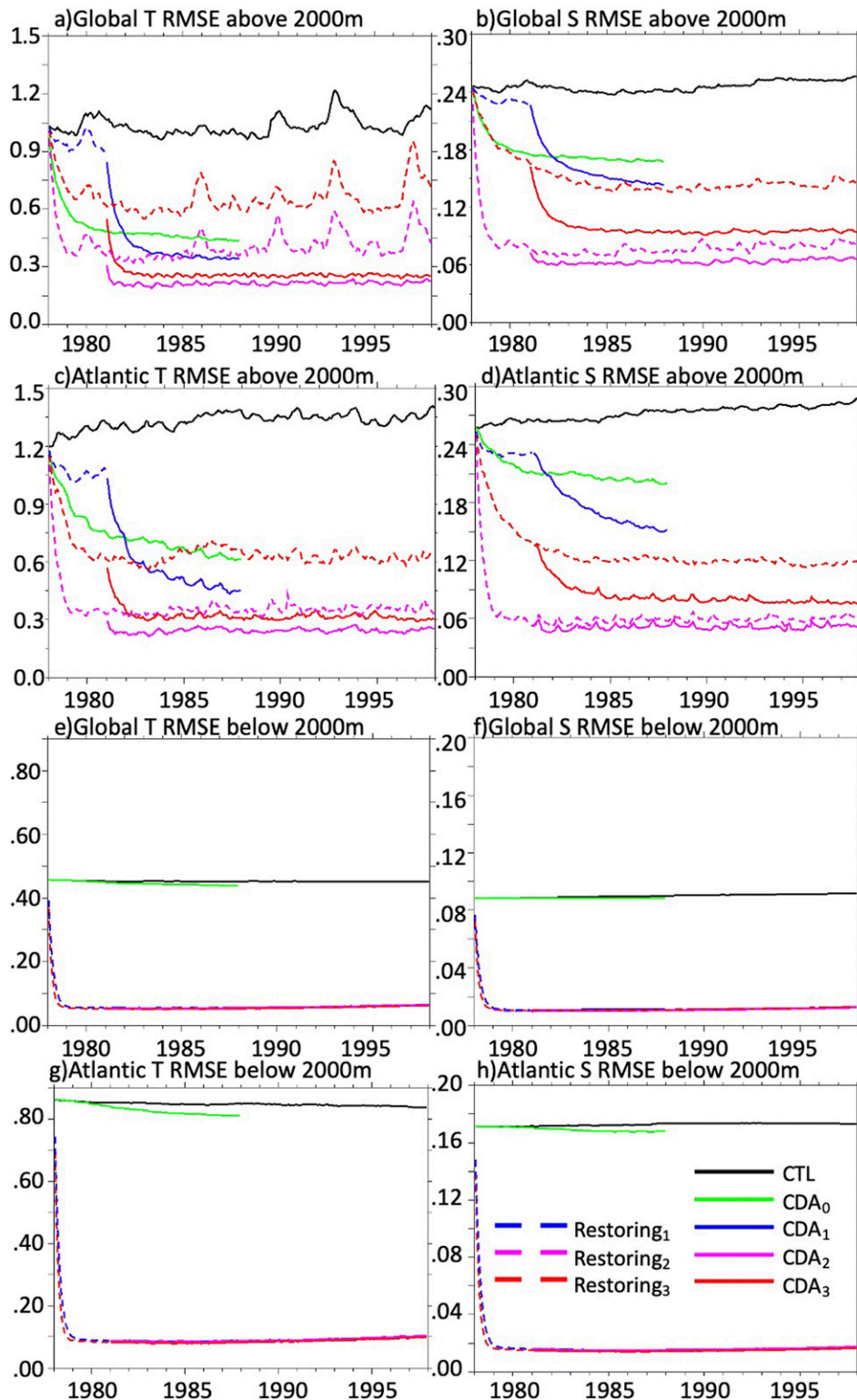
FIG. 5. The root-mean-square error (RMSE) with respect to CESM1.3 "truth" (a)–(d) above and (e)–(h) below 2000 m of (a),(b),(e),(f) the global ocean and (c),(d),(g),(h) the Atlantic Ocean (left) temperature (°C) and (right) salinity (psu) in CTL (black line, CM2.1 free run), CDA_0 (green line, with CDA only), $Restoring_1$ (dashed blue line, with T and S restoring below 1000 m), CDA_1 (solid blue line, CDA with $Restoring_1$), $Restoring_2$ (dashed purple line, with T and S restoring in all ocean layers), CDA_2

of the bias between numerical models and the real world. In addition, the AMOC variabilities in CESM1.3 and CM2.1 are largely independent with a correlation coefficient of only 0.25 between the monthly-mean time series (further studies may be interesting to attribute the correlation to a common seasonal cycle or external forcing). These systematic differences in mean state and variability must be associated with many features in the AMOC system such as the different modeling capability to simulate key strait overflows (e.g., Denmark Strait and Faroe Bank Channel) (Danabasoglu et al. 2010).

a. Convergent upper-ocean temperature and salinity in CDA_0

The first reconstruction experiment is CDA_0, in which the CM2.1-ECDA system described in section 2a(3) assimilates the "observations" of ocean temperature and salinity, as well as atmospheric temperature and wind produced by CESM1.3. The root-mean-square errors (RMSEs) of ocean temperature and salinity above (below) 2000 m are shown in Fig. 5 as green lines (Figs. 5a,b,e,f are for the global ocean and Figs. 5c,d,g,h are for the Atlantic). Figure 5 shows that the assimilation system works well, with the observations successfully assimilated into the coupled model. After the 3-yr assimilation spinup, the assimilated ocean states over the upper 2000 m converge toward the "truth."

Since the state of AMOC could be influenced by the atmospheric forcing in a coupled system, we use Fig. 6 to confirm the atmosphere data assimilation (ADA) does work to constrain the CM2 model to the data produced by the CESM1.3 model. Figure 6 shows that through a few days of ADA constraints, the RMSEs of CM2 atmosphere temperature and wind reduce greatly (by 70% and 50%, respectively), and after about 10 days, the ADA reaches the equilibrium. While the impact of atmospheric high-frequency constraints on the AMOC analysis will be thoroughly examined in follow-up studies, we will focus on the influence of ocean stratification in ODA on the AMOC reconstruction in this study.

b. Misrepresentation of the AMOC mean state

We use the CDA_0 results over years 4–10 to calculate the AMOC mean state, seasonal cycle, and variability (Fig. 7). Surprisingly, we find that, although the surface forcing from the atmosphere and upper-2000-m ocean

temperature and salinity are constrained, the resulting AMOC is totally misrepresented. The AMOC lower cell becomes much stronger, with the zero contour reaching 1000-m depth at ~20°N. This leads to a much shallower NADW and a broader AABW in CDA_0 compared with that in either the CESM simulation or the original CM2.1 simulation, as shown in Fig. 4. The seasonal cycle and variability are also degraded compared with the CM2.1 model control (Figs. 4b,c).

To understand the reasons for AMOC misrepresentation in CDA_0, in Fig. 8 we examine the time-varying relative RMSE normalized by the RMSE of CM2.1 CTL ($RMSE_{CDA}/RMSE_{CTL}$) of ocean temperature, salinity, and density in depth–time space in Atlantic. Due to utilization of the adaptive inflation ensemble filter (AIEF) scheme (Zhang et al. 2010), the assimilation of Argo data in CDA_0 leads to an improvement in ocean temperature and salinity down to 2500-m depth (i.e., $RMSE_{CDA}/RMSE_{CTL} < 1$). The improvement of ocean temperature is much greater than that of salinity (the relative RMSE of temperature is smaller than that of salinity). However, while the ocean temperature and salinity show clear improvement in the upper 2500 m, the density is improved only in the upper 600 m. At deeper levels, density gets even worse ($RMSE_{CDA}/RMSE_{CTL} > 1$). It seems that, due to the model bias of CM2.1 with respect to CESM1.3, when only the upper ocean is constrained by the "observed" data, the biased model develops incoherent ocean stratification (too-light water between 500 and 3000 m in the Atlantic; dashed cyan line in Fig. 9b). The instability associated with such erroneous stratification of the ocean column causes the AABW cell to strengthen and expand, leading to misrepresentation of the AMOC.

Next, we will examine further experiments designed to enhance the coherence of ocean stratification so as to improve the AMOC structure.

4. Importance of coherent ocean stratification for AMOC reconstruction

a. Mean state

Considering that observations below 2000 m are very sparse and internal variability in the deep ocean is weak, we employ global climatological restoring of temperature and salinity (e.g., Levitus et al. 2001, 2005, 2012) in

---

←

(solid purple line, CDA with Restoring₂), Restoring₃ (dashed red line, with T and S restoring in all ocean layers but lighter restoring above and stronger restoring below 1500 m relative to Restoring₂), and CDA_3 (solid red line, CDA with Restoring₃). See Table 1 for detailed descriptions of all experiments. Note that to save computational resources, CDA_0 and CDA_1 are only run for the first 10 years.
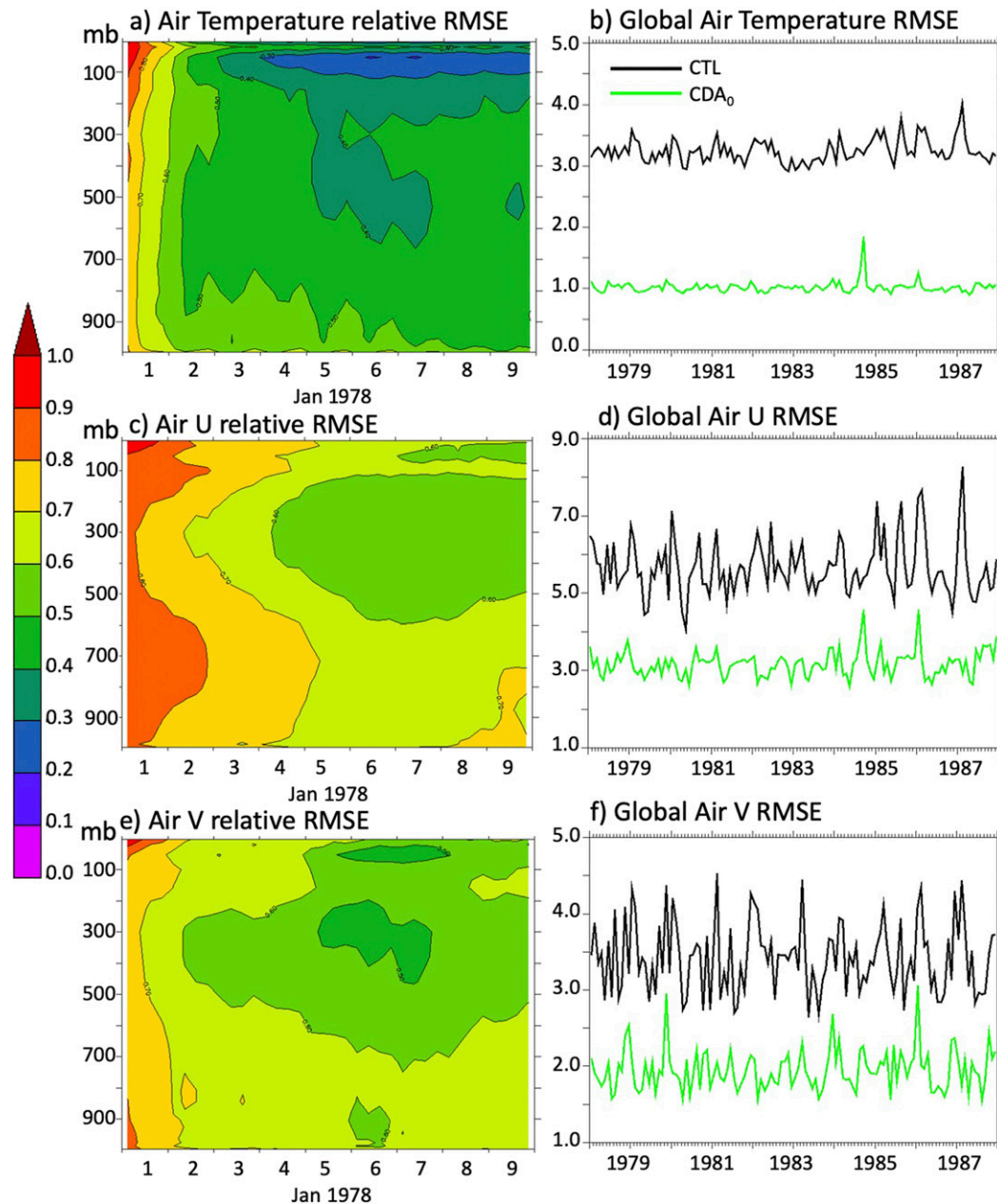
FIG. 6. Time series of (a),(c),(e) the horizontally averaged relative root-mean-square errors ($RMSE_{CDA0}/RMSE_{CTL}$) with the assimilation days and (b),(d),(f) the global root-mean-square errors (RMSEs) with the assimilation years of (a),(b) air temperature (K), (c),(d) zonal wind U (m s^{-1}), and (e),(f) meridional wind V (m s^{-1}) of CDA_0. In (a), (c), and (e), the time frequency is 6 h to show the process of RMSE reduction in CDA_0 from the CTL. In (b), (d), and (f), the green (black) line is the CDA_0 (CTL) against the "TRUTH" (CESM1.3).

the deep ocean to relax the distorted ocean stratification (caused by strong data constraint in upper ocean, shown in Figs. 8c, 9a, and 9b) with an inconsistent ocean vertical structure causing instability. We first construct the climatology using ocean temperature and salinity from the CESM "truth" simulation. Then we restore the CM2.1 toward this climatology for 3 years with the restoring scheme depicted by the green line in Fig. 10 (called "Restoring$_1$" in Table 1). The Restoring$_1$ scheme nudges CM2.1 toward the "truth" climatology of temperature and salinity data starting from 1000 m ramping to a 180-day (0.64×10^{-7} s^{-1}) restoring time scale at 1500 m, and eventually extends to a 60-day (1.93×10^{-7} s^{-1}) time scale at the bottom. For optimal utilization
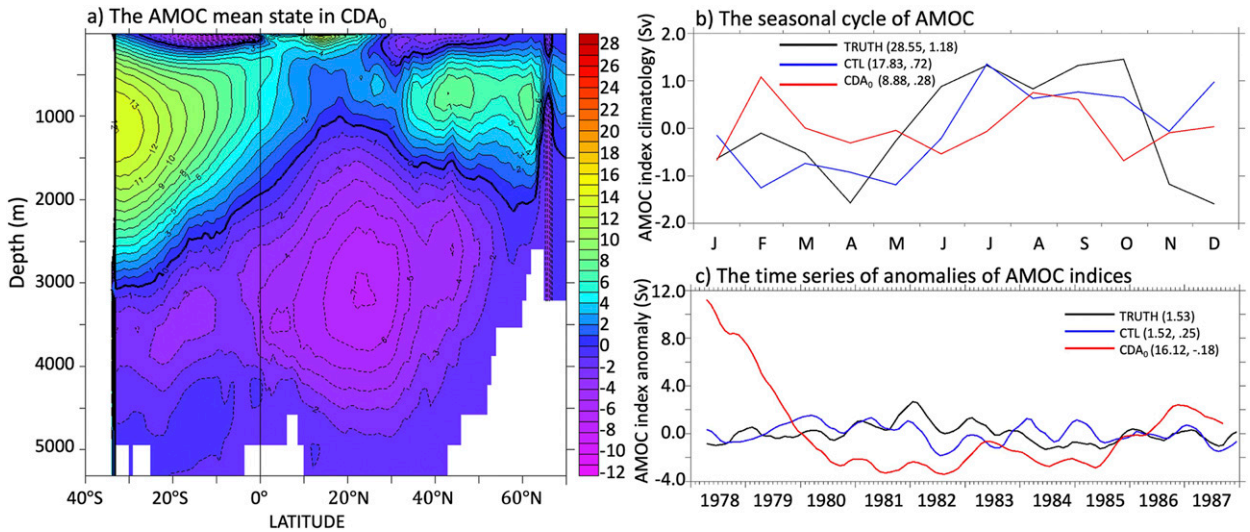
FIG. 7. (a) The CDA$_0$ AMOC mean state (1981–87) and (b) the climatology and (c) the anomaly time series (six-point smoothing) of AMOC indices produced by CM2.1 CDA$_0$ (red) and CTL (blue) as well as the CESM "TRUTH" run (black). The two numbers in parentheses in the legend in (b) are the annual mean value and climatological variance, respectively, and the two numbers in parentheses in the legend in (c) are the anomaly variance and correlation coefficient with the "truth," respectively.

of computational resource, we start the CDA experiment (called CDA$_1$) after the model gets sufficient restoring spinup. Here, the CDA$_1$ is initialized from the coupled model states at the end of the 3-yr restoring spinup (i.e., at 0000 UTC 1 January 1981) and is then run forward with the Restoring$_1$ scheme.

The RMSEs of ocean temperature and salinity from Restoring$_1$ and the follow-up CDA$_1$ are plotted in Fig. 5

as dashed (Restoring$_1$) and solid (CDA$_1$) lines. Based on Restoring$_1$, CDA$_1$ further reduced the errors of ocean temperature and salinity, especially for the deep ocean below 2000 m. Furthermore, from the time-varying relative RMSE (i.e., RMSE$_{CDA1}$/RMSE$_{CTL}$) of density in CDA$_1$ (see Fig. 11a), we see that the CDA$_1$ improves the density structure below 600-m depth compared to CDA$_0$ (cf. Figs. 11a and 8c), with a maximal reduction in the
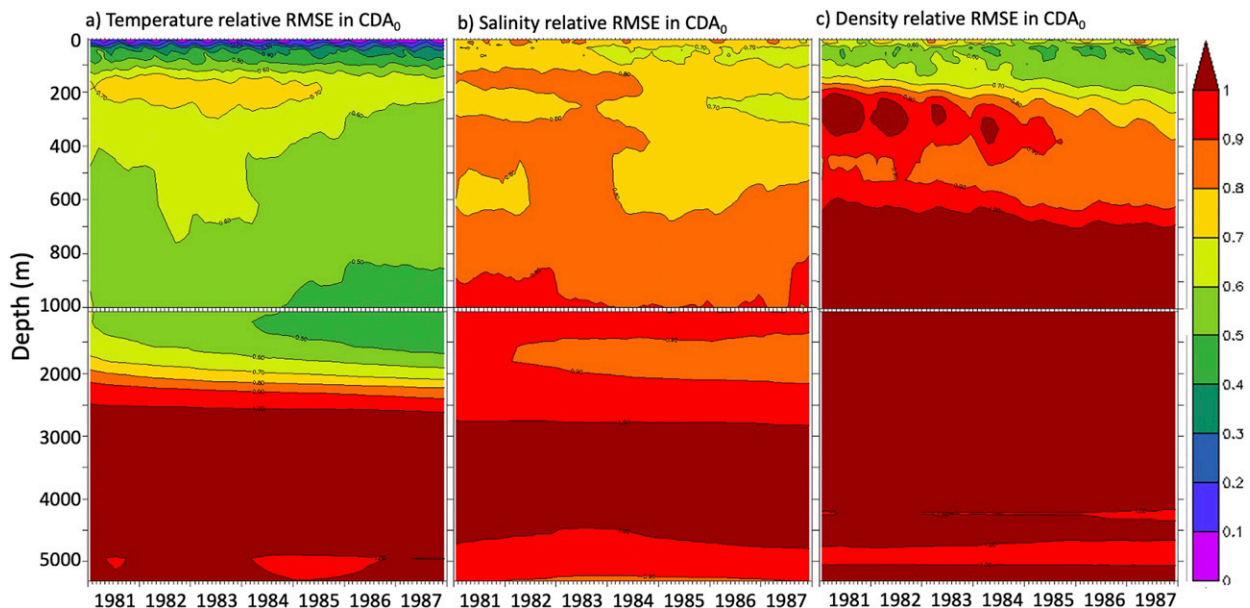

FIG. 8. The distribution of the relative RMSE (RMSE$_{CDA}$/RMSE$_{CTL}$) of the Atlantic Ocean (a) temperature, (b) salinity, and (c) density in depth–time space produced by CDA$_0$. The areas with the values of RMSE$_{CDA}$/RMSE$_{CTL}$ < 1 (> 1) indicate improvement (degradation) by the assimilation. For visualization, above (below) 1000 m the vertical interval is 100 (500) m.
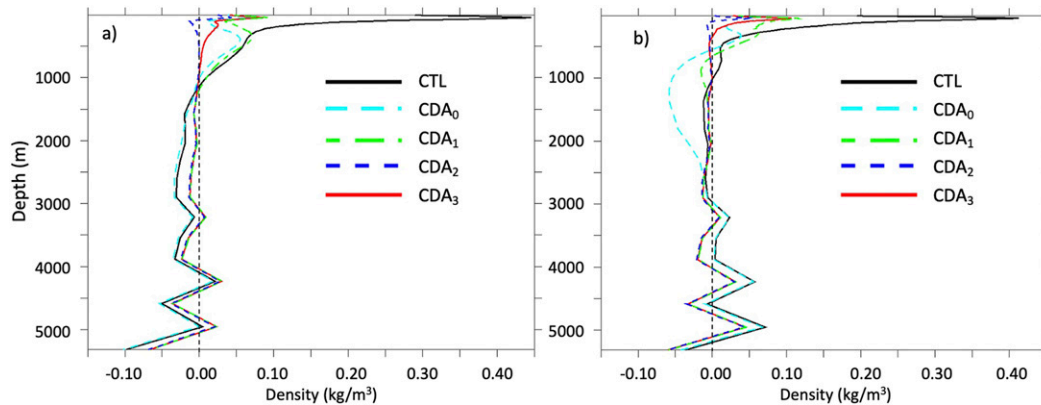
FIG. 9. Profiles of density bias (time-averaged global mean error) in (a) the global ocean and (b) the Atlantic Ocean of CTL (solid black), CDA_0 (dashed cyan), CDA_1 (dashed green), CDA_2 (dashed blue), and CDA_3 (solid red).

density error reaching 50% below 1000 m. With much improved ocean stratification, the major distortion of the AMOC mean state vanishes (cf. Figs. 12a and 7a). Compared with CDA_0, the AMOC structure in CDA_1 is much closer to the "truth" simulated by the CESM model (cf. Figs. 12a and 4a), although large differences still remain.

Using the $Restoring_1$ scheme, in which restoring is conducted below 1000 m, we can see that the structure of the CDA_1-reconstructed AMOC mean state and seasonal cycle as well as its variability, especially the strength of the mean state, are more reasonable than those in CDA_0 (Figs. 12b,c), meaning that mitigation of model bias could reduce the artifacts in the assimilation variability (e.g., Dee 2005; Zhang et al. 2012). However, the CDA_1 AMOC strength (annual mean value of 16 Sv) is still much weaker than the "truth" (annual mean

value of 29 Sv), and indeed weaker than that in the CM2.1 CTL (annual mean value of 18 Sv). This may be because, between 200 and 1000 m, the relative RMSEs of CDA_1 for density remain large (Fig. 11a). In the $Restoring_2$ experiment, we extend the climatology restoring time scale of 180 days at 1500 m to the surface (dashed blue line in Fig. 10; Table 1). This experiment is run for 3 years starting from 0000 UTC 1 January 1978 and then used to initialize a CDA experiment, CDA_2. With the addition of $Restoring_2$, CDA_2 improves the density structure between 200 and 1000 m from CDA_1 (cf. Fig. 11b with Fig. 11a). The resulting AMOC mean state and seasonal cycle, as well as its variability, are plotted in Fig. 13. As a result of restoring to climatology above 1000 m, the AMOC mean state of CDA_2 becomes much stronger, with the annual mean value increasing to 23 Sv.

b. Variability

From the above analyses of the results of the three CDA experiments, it is clear that we can use climatological restoring of ocean temperature and salinity to improve the estimates of AMOC mean state and seasonal cycle. However, based on a comparison of Fig. 13c with Fig. 12c, we find that while the climatology restoring at upper oceans enhances the AMOC strength, it tends to damp AMOC variability. Meanwhile, Fig. 11b indicates that with $Restoring_2$ the density errors in the deep ocean below 1000 m remain large and increase with depth. These results suggest that the upper-ocean climatology restoring may be too strong so that variability is damped too much, while the deep-ocean restoring is too weak. To further increase the coherence of the ocean stratification for sustaining AMOC variability, we design a new restoring scheme, $Restoring_3$ that basically strengthens (weakens) the deep-ocean (upper-ocean)
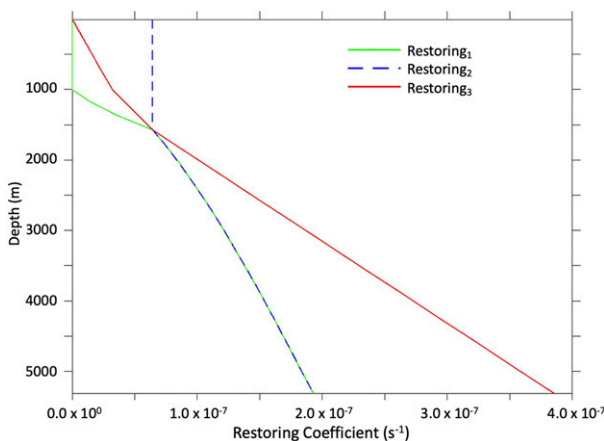

FIG. 10. Depth dependence of the restoring coefficients (s^{-1}) used in the $Restoring_1$ (green), $Restoring_2$ (dashed blue), and $Restoring_3$ (red) schemes listed in Table 1.
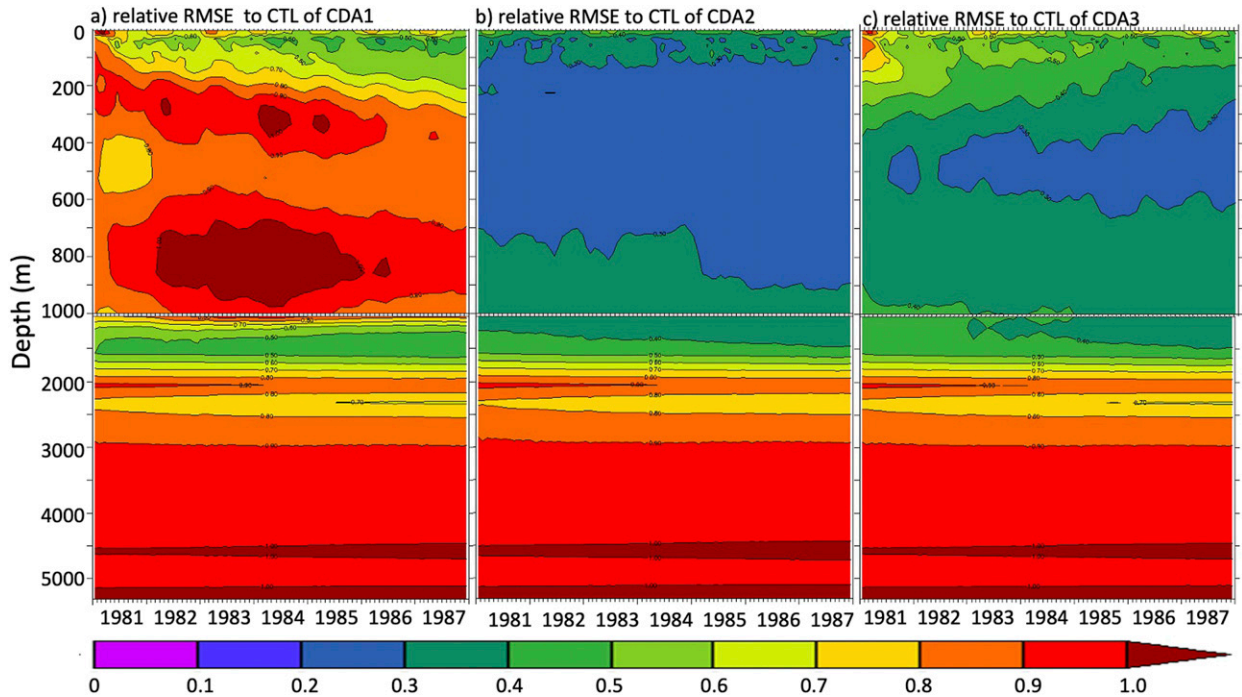
FIG. 11. As in Fig. 8c, but for (a) CDA$_1$ (assimilating ocean temperature and salinity "observations" with the Restoring$_1$ scheme), (b) CDA$_2$ (assimilating ocean temperature and salinity "observations" with the Restoring$_2$ scheme), and (c) CDA$_3$ (assimilating ocean temperature and salinity "observations" with the Restoring$_3$ scheme) (see Table 1).

restoring. As shown by the red line of Fig. 10, the restoring time scales ramp from the surface to 1000 m as 0 to 360 days, from 1000 to 1500 m as 360 to 180 days, and from 1500 m to the bottom as 180 to 30 days. Following the same approach as in CDA$_1$ and CDA$_2$, we conduct a new experiment called CDA$_3$. The relative RMSEs of

density in depth–time space are plotted in Fig. 11c, with the AMOC mean state and seasonal cycle, as well as its variability, shown in Fig. 14.

With the weaker relaxation (restoring) to the upper-ocean climatology in CDA$_3$, variability of the reconstructed AMOC is much improved, with the correlation and variance
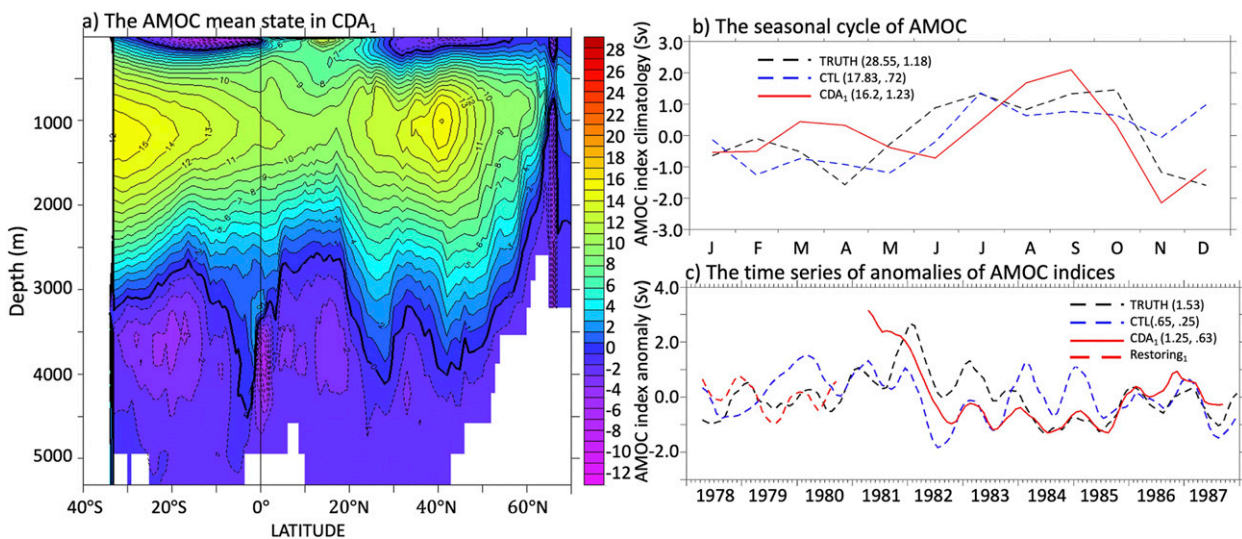

FIG. 12. As in Fig. 7, but for CDA$_1$. The variance and correlation coefficient between CTL or CDA$_1$ and TRUTH AMOC anomalies are calculated using the data from the last 7 years (1981–87).
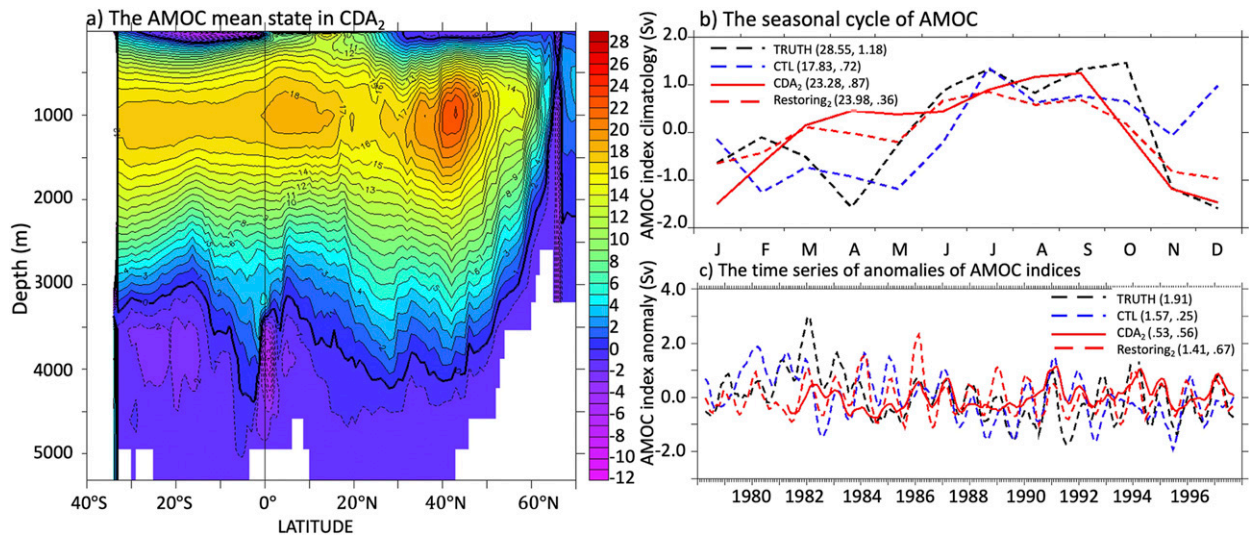
FIG. 13. As in Fig. 7, but for CDA$_2$. The statistics are based on the data of the last 10 years (1988–97).

increasing up to 0.78 and 1.56 from 0.56 and 0.37 in CDA$_2$, respectively, which are also improved compared to Restoring$_3$ (0.67 and 1.28 as correlation and variance, respectively). These results suggest that in order to have AMOC well represented, it is very important to have sound restoring to sustain the mean state of AMOC working with instantaneous data assimilation which retrieves "high"-frequency AMOC variability. This could have important implications for designing assimilation systems for, e.g., decadal predictions.

5. Summary and discussion

Due to different model biases, the reconstructed AMOCs obtained by combining coupled models and observations in

different reanalyses products show highly divergent characteristics (Karspeck et al. 2015; Jackson et al. 2019). In this work, a biased twin experiment framework is designed to study the influence of model bias on AMOC reconstruction. The biased twin experiments consist of two independent coupled general circulation models (CGCMs), GFDL CM2.1 and NCAR CESM1.3, and a coupled ensemble filter with GFDL CM2.1. Based on the modern climate observing system (Argo temperature and salinity profiles as well as SST for the ocean, and reanalysis gridded data of temperature and wind for the atmosphere), the atmosphere and ocean "observations" are drawn from a CESM historical simulation that defines the "true" solution of the CDA problem. Then, the synthetic observations are assimilated into the CM2.1 by the ensemble
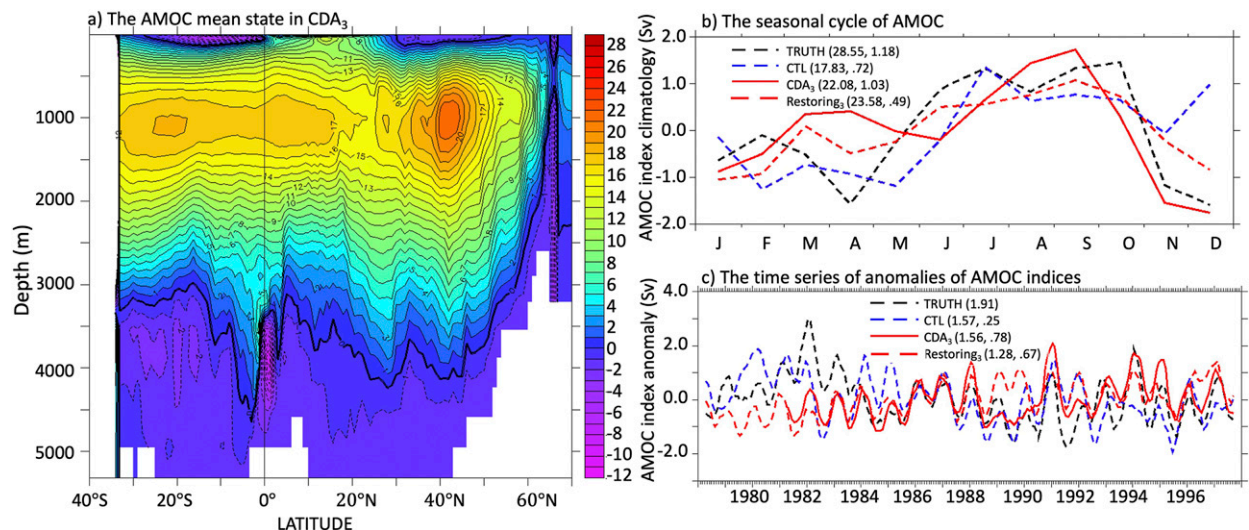

FIG. 14. As in Fig. 13, but for CDA$_3$.

filter to recover the "truth." The degree to which the true AMOC state is recovered in different CDA schemes that deal with the model bias differently provides insight into the influence of model bias on AMOC reconstruction.

Our results show that while the traditional CDA system effectively assimilates the atmosphere and upper-ocean "observations" into the coupled model and reduces upper-ocean errors significantly, the reconstructed AMOC becomes totally distorted in both the mean structure and variability due to incoherent ocean density stratification in our experiments. Given that most of ocean observations are only available in the upper ocean (above 2000 m), it is necessary to enhance the coherence of ocean vertical structure in ocean data assimilation. Here we examine revised CDA schemes that include climatological restoring of ocean temperature and salinity to assess the AMOC analyses when the ocean vertical structure is improved. In general, restoring to climatology can greatly reduce the ocean model bias and improve the coherence of ocean vertical structure, thus improving estimates of the AMOC mean state. However, excessively strong restoring in the upper ocean can degrade the reconstruction of AMOC variability. A sound CDA scheme that has a balance between the climatological restoring and the instantaneous data constraints gives the most accurate reconstruction of AMOC structure and variability. Given the relatively independent nature of the CESM versus CM2 models, the main conclusion gained in this study may have implication for other CMIP5 models, although we use the CESM as the "truth" model that produces the "observations."

Reconstructing the historical mean structure and variability of AMOC based on observational information is an important step in understanding the large-scale variability of the global climate (e.g., Delworth and Dixon 2000, 2006; Zhang et al. 2009, 2010). This study serves as a guide for combining the Earth observing system with a CGCM to reconstruct twentieth-century AMOC. Our results suggest that for a given CGCM, with its own bias characteristics, an appropriate climatological restoring scheme in the ocean model working with the CDA system is of critical importance. However, due to the rich spectrum of AMOC variability associated with various complex mechanisms, many other factors need to be considered in order to generate accurate and robust AMOC state estimates using observations combined with models. For example, how do high-frequency air–sea interactions in the tropical Atlantic impact AMOC structure and variability? Given the close relation between sea ice and AMOC, what is the impact of sea ice observational constraints on the AMOC reconstruction? Another obvious follow-up would be to apply the setup of this study to the twentieth-century observing system to learn what could be expected as the

first step that attempts to produce an historical AMOC reconstruction. Given that deep Argo deployment has begun (https://www.climate.gov/news-features/climate-tech/deep-argo-diving-answers-ocean%E2%80%99s-abyss), in the future with improved model parameterizations (for key strait overflows, for instance), accurately estimating and predicting the AMOC state to some degree is feasible.

REFERENCES

Anderson, J. L., 2001: An ensemble adjustment Kalman filter for data assimilation. *Mon. Wea. Rev.*, **129**, 2884–2903, https://doi.org/10.1175/1520-0493(2001)129<2884:AEAKFF>2.0.CO;2.

——, 2003: A local least squares framework for ensemble filtering. *Mon. Wea. Rev.*, **131**, 634–642, https://doi.org/10.1175/1520-0493(2003)131<0634:ALLSFF>2.0.CO;2.

Balmaseda, M. A., D. P. Dee, A. Vidard, and D. L. T. Anderson, 2007: A multivariate treatment of bias for sequential data assimilation: Application to the tropical oceans. *Quart. J. Roy. Meteor. Soc.*, **133**, 167–179, https://doi.org/10.1002/qj.12.

Buckley, M. W., and J. Marshall, 2016: Observations, inferences, and mechanisms of the Atlantic meridional overturning circulation: A review. *Rev. Geophys.*, **54**, 5–63, https://doi.org/10.1002/2015RG000493.

Chepurin, G. A., J. A. Carton, and D. Dee, 2005: Forecast model bias correction in ocean data assimilation. *Mon. Wea. Rev.*, **133**, 1328–1342, https://doi.org/10.1175/MWR2920.1.

Danabasoglu, G., W. G. Large, and B. P. Briegleb, 2010: Climate impacts of parameterized Nordic Sea overflows. *J. Geophys. Res.*, **115**, C11005, https://doi.org/10.1029/2010JC006243.

——, and Coauthors, 2014: North Atlantic simulations in Coordinated Ocean-ice Reference Experiments phase II (CORE-II). Part I: Mean states. *Ocean Modell.*, **73**, 76–107, https://doi.org/10.1016/j.ocemod.2013.10.005.

Dee, D. P., 2004: Variational bias correction of radiance data in the ECMWF system. *Proc. ECMWF Workshop on Assimilation of High Spectral Resolution Sounders in NWP*, Reading, United Kingdom, ECMWF, 97–112.

——, 2005: Bias and data assimilation. *Quart. J. Roy. Meteor. Soc.*, **131**, 3323–3343, https://doi.org/10.1256/qj.05.137.

——, and A. M. da Silva, 1998: Data assimilation in the presence of forecast bias. *Quart. J. Roy. Meteor. Soc.*, **124**, 269–295, https://doi.org/10.1002/qj.49712454512.

Delworth, T. L., and K. W. Dixon, 2000: Implications of the recent trend in the Arctic/North Atlantic Oscillation for the North Atlantic thermohaline circulation. *J. Climate*, **13**, 3721–3727, https://doi.org/10.1175/1520-0442(2000)013<3721:IOTRTI>2.0.CO;2.

——, and ——, 2006: Have anthropogenic aerosols delayed a greenhouse gas-induced weakening of the North Atlantic thermohaline circulation? *Geophys. Res. Lett.*, **33**, L02606, https://doi.org/10.1029/2005GL024980.

——, S. Manabe, and R. J. Stouffer, 1993: Interdecadal variations of the thermohaline circulation in a coupled ocean–atmosphere model. *J. Climate*, **6**, 1993–2011, https://doi.org/10.1175/1520-0442(1993)006<1993:IVOTTC>2.0.CO;2.

——, R. J. Stouffer, K. W. Dixon, M. J. Spelman, T. R. Knutson, A. J. Broccoli, P. J. Kushner, and R. T. Wetherald, 2002: Review of simulations of climate variability and change with the GFDL R30 coupled climate model. *Climate Dyn.*, **19**, 555–574, https://doi.org/10.1007/s00382-002-0249-5.

——, and Coauthors, 2006: GFDL's CM2 global coupled climate models. Part I: Formulation and simulation characteristics. *J. Climate*, **19**, 643–674, https://doi.org/10.1175/JCLI3629.1.

——, and Coauthors, 2008: The potential for abrupt change in the Atlantic meridional overturning circulation. *Abrupt Climate Change*, U.S. Geological Survey, 258–359, https://opensky.ucar.edu/islandora/object/books%3A255.

Frierson, D. M. W., and Coauthors, 2013: Contribution of ocean overturning circulation to tropical rainfall peak in the Northern Hemisphere. *Nat. Geosci.*, **6**, 940–944, https://doi.org/10.1038/ngeo1987.

Gnanadesikan, A., and Coauthors, 2006: GFDL's CM2 global coupled climate models. Part II: The baseline ocean simulation. *J. Climate*, **19**, 675–697, https://doi.org/10.1175/JCLI3630.1.

Hurrell, J. W., and Coauthors, 2013: The Community Earth System Model: A framework for collaborative research. *Bull. Amer. Meteor. Soc.*, **94**, 1339–1360, https://doi.org/10.1175/BAMS-D-12-00121.1.

Jackson, L. C., and Coauthors, 2019: The mean state and variability of the North Atlantic circulation: A perspective from ocean reanalyses. *J. Geophys. Res. Oceans*, **124**, 9141–9170, https://doi.org/10.1029/2019JC015210.

Johns, W. E., and Coauthors, 2011: Continuous, array-based estimates of Atlantic ocean heat transport at 26.5°N. *J. Climate*, **24**, 2429–2449, https://doi.org/10.1175/2010JCLI3997.1.

Karspeck, A. R., and Coauthors, 2015: Comparison of the Atlantic meridional overturning circulation between 1960 and 2007 in six ocean reanalysis products. *Climate Dyn.*, **49**, 957–982, https://doi.org/10.1007/s00382-015-2787-7.

Keenlyside, N. S., M. Latif, J. Jungclaus, L. Kornblueh, and E. Roeckner, 2008: Advancing decadal-scale climate prediction in the North Atlantic sector. *Nature*, **453**, 84–88, https://doi.org/10.1038/nature06921.

Levitus, S., T. Boyer, M. Concright, D. Johnson, T. O'Brien, J. Antonov, C. Stephens, and R. Garfield, 1998: Introduction. Vol. I, *World Ocean Database 1998*, NOAA Atlas NESDIS 18, 346 pp.

——, J. I. Antonov, J. Wang, T. L. Delworth, K. W. Dixon, and A. J. Broccoli, 2001: Anthropogenic warming of Earth's climate system. *Science*, **292**, 267–270, https://doi.org/10.1126/science.1058154.

——, ——, and T. P. Boyer, 2005: Warming of the world ocean, 1955–2003. *Geophys. Res. Lett.*, **32**, L02604, https://doi.org/10.1029/2004GL021592.

——, and Coauthors, 2012: World ocean heat content and thermosteric sea level change (0–2000 m), 1955–2010. *Geophys. Res. Lett.*, **39**, L10603, https://doi.org/10.1029/2012GL051106.

Lin, S.-J., 2004: A "vertically Lagrangian" finite-volume dynamical core for global models. *Mon. Wea. Rev.*, **132**, 2293–2307, https://doi.org/10.1175/1520-0493(2004)132<2293:AVLFDC>2.0.CO;2.

Macdonald, A., and M. Baringer, 2013: Observed ocean transport of heat. *Ocean Circulation and Climate: A 21st Century Perspective*, G. Siedler et al., Eds., Elsevier, 759–785.

Mahajan, S., R. Zhang, T. L. Delworth, S. Zhang, A. J. Rosati, and Y.-S. Chang, 2011: Predicting Atlantic meridional overturning circulation (AMOC) variations using subsurface and surface fingerprints. *Deep-Sea Res. II*, **58**, 1895–1903, https://doi.org/10.1016/j.dsr2.2010.10.067.

Marshall, J., A. Donohoe, D. Ferreira, and D. McGee, 2014: The ocean's role in setting the mean position of the inter-tropical convergence zone. *Climate Dyn.*, **42**, 1967–1979, https://doi.org/10.1007/s00382-013-1767-z.

Randall, D. A., and Coauthors, 2007: Climate models and their evaluation. *Climate Change 2007: The Physical Science Basis*, S. Solomon et al., Eds., Cambridge University Press, 589–662.

Steele, M., R. Morley, and W. Ermold, 2001: PHC: A global ocean hydrography with a high-quality Arctic Ocean. *J. Climate*, **14**, 2079–2087, https://doi.org/10.1175/1520-0442(2001)014<2079:PAGOHW>2.0.CO;2.

Taylor, K. E., R. J. Stouffer, and G. A. Meehl, 2012: An overview of CMIP5 and the experiment design. *Bull. Amer. Meteor. Soc.*, **93**, 485–498, https://doi.org/10.1175/BAMS-D-11-00094.1.

Yeager, D. S., M. D. Henderson, D. Paunesku, G. M. Walton, S. D'Mello, B. J. Spitzer, and A. L. Duckworth, 2014: Boring but important: A self-transcendent purpose for learning fosters academic self-regulation. *J. Pers. Soc. Psychol.*, **107**, 559–580, https://doi.org/10.1037/a0037637.

Zhang, S., and A. Rosati, 2010: An inflated ensemble filter for ocean data assimilation with a biased coupled GCM. *Mon. Wea. Rev.*, **138**, 3905–3931, https://doi.org/10.1175/2010MWR3326.1.

——, M. J. Harrison, A. T. Wittenberg, A. Rosati, J. L. Anderson, and V. Balaji, 2005: Initialization of an ENSO forecast system using a parallelized ensemble filter. *Mon. Wea. Rev.*, **133**, 3176–3201, https://doi.org/10.1175/MWR3024.1.

——, ——, A. Rosati, and A. Wittenberg, 2007: System design and evaluation of coupled ensemble data assimilation for global oceanic climate studies. *Mon. Wea. Rev.*, **135**, 3541–3564, https://doi.org/10.1175/MWR3466.1.

——, A. Rosati, and M. J. Harrison, 2009: Detection of multidecadal oceanic variability by ocean data assimilation in the context of a "perfect" coupled model. *J. Geophys. Res.*, **114**, C12018, https://doi.org/10.1029/2008JC005261.

——, ——, and T. Delworth, 2010: The adequacy of observing systems in monitoring the Atlantic meridional overturning circulation and North Atlantic climate. *J. Climate*, **23**, 5311–5324, https://doi.org/10.1175/2010JCLI3677.1.

——, Z. Liu, A. Rosati, and T. Delworth, 2012: A study of enhancive parameter correction with coupled data assimilation for climate estimation and prediction using a simple coupled model. *Tellus*, **64A**, 10963, https://doi.org/10.3402/tellusa.v64I0.10963.

——, Y.-S. Chang, X. Yang, and A. Rosati, 2014: Balanced and coherent climate estimation by combining data with a biased coupled model. *J. Climate*, **27**, 1302–1314, https://doi.org/10.1175/JCLI-D-13-00260.1.